Journal Pre-proof

Comparative study of CO_2 hydrogenation to methanol on cubic bixbyite-type and rhombohedral corundum-type indium oxide

Bin Yang, Longtai Li, Ziye Jia, Xiping Liu, Chunjie Zhang, Limin Guo

PII: S1001-8417(20)30316-8

DOI: https://doi.org/10.1016/j.cclet.2020.05.031

Reference: CCLET 5669

To appear in: *Chinese Chemical Letters*

Received Date: 15 April 2020

Revised Date: 9 May 2020

Accepted Date: 21 May 2020

Please cite this article as: Yang B, Li L, Jia Z, Liu X, Zhang C, Guo L, Comparative study of CO_2 hydrogenation to methanol on cubic bixbyite-type and rhombohedral corundum-type indium oxide, *Chinese Chemical Letters* (2020), doi: https://doi.org/10.1016/j.cclet.2020.05.031

Communication

Comparative study of CO_2 hydrogenation to methanol on cubic bixbyite-type and rhombohedral corundum-type indium oxide

Bin Yang[a], Longtai Li[a], Ziye Jia[a], Xiping Liu[b], Chunjie Zhang[b], Limin Guo[a,*]

[a] *School of Environmental Science and Engineering, Huazhong University of Science and Technology, Wuhan 430074, China*
[b] *Research Institute of Air Purification Equipment, Shanxi Xinhua Chemical Co., LTD, Taiyuan 03008, China*

∗ Corresponding author. Tel: +86-2787792101
E-mail address: lmguo@hust.edu.cn (L. Guo).

Graphical Abstract

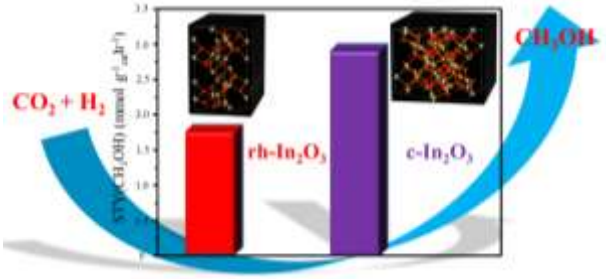

The cubic bixbyite-type In_2O_3 showed higher CH_3OH productivity than rhombohedral corundum-type In_2O_3 due to the impressive reducibility and reactivity. Further characterization indicated the identical catalytic mechanism, CO_2 can be reduced to CO through redox cycling and hydrogenation to CH_3OH through formate path.

ARTICLE INFO

Article history:
Received 15 April 2020
Received in revised form 9 May 2020
Accepted 15 May 2020
Available online

Keywords:
CO_2 hydrogenation;
In_2O_3
Methanol
Structure effect.

ABSTRACT

Hydrogenation of CO_2 to value-added chemicals has attracted much attention all through the world. In_2O_3 with cubic bixbyite-type (denoted as c-In_2O_3) is well known for its high CO_2 hydrogenation activity and CH_3OH selectivity at high temperature. However, the other structure of In_2O_3 with rhombohedral corundum-type (denoted as rh-In_2O_3) rarely been investigated as catalyst. Herein, c-In_2O_3 and rh-In_2O_3 were prepared and comparatively studied for CO_2 hydrogenation. The results indicated that c-In_2O_3 showed higher CO_2 conversion activity than rh-In_2O_3 due to the impressive reducibility and reactivity. Whereas rh-In_2O_3 had higher CH_3OH selectivity due to weaker CH_3OH and stronger CO adsorption on rh-In_2O_3. Although c-In_2O_3 and rh-In_2O_3 catalysts showed different CO_2 hydrogenation performance, *in-situ* diffuse reflectance infrared Fourier transform spectroscopy showed CO_2 can be reduced to CO through redox cycling and hydrogenation to CH_3OH through formate path.

CO_2 emission caused by human activities results in global warming and ecological issues [1,2]. The conversion of CO_2 into value-added hydrocarbon is a promising way to eliminate CO_2 [3]. Hydrogenation of CO_2 to methanol (CH_3OH) is one of the most promising approaches for its transformation [1,4]. Moreover, CH_3OH can be directly used to synthesize olefin and high value-added hydrocarbons through zeolite catalysis [5-8]. By coupling of methanol-synthesis and methanol-to-hydrocarbons reaction with a bifunctional catalyst can realize the direct conversion of CO_2 to hydrocarbon products, *e.g.* gasoline(C_5-C_{11}), lower olefin(C_2-C_4) and aromatic hydrocarbon [5,9]. It contains two consecutive processes: methanol synthesis from CO_2 through metal-oxide catalysts and methanol to hydrocarbons through zeolites catalysts [10]. It is an essential prerequisite that the reaction temperature of methanol to hydrocarbons should be over 340 °C [9,10], which is thermodynamically restrained for methanol synthesis from CO_2 and H_2. The CH_3OH selectivity of conventionally Cu-based catalysts is lower than 5% over 320 °C [5,7]. Obviously, significant and effective catalysts are required for this strategy. As Oliver Martin reported, the methanol selectivity of In_2O_3 with cubic bixbyite-type can be tuned up to 100% from 200 °C to 300 °C and over 25% at 340 °C, which was closed to thermodynamic limit [11,12]. Further researches showed In_2O_3 had emerged as an outstanding catalytic system for CO_2 hydrogenation to methanol with highly selectivity under industrially relevant conditions [12].

In_2O_3 is known as a conductive transparent layer and thin-film transistors [13,14]. There are two representative crystal structures, namely cubic bixbyite-type (denoted as c-In_2O_3) and rhombohedral corundum-type (denoted as rh-In_2O_3) [14]. As the most studied structure, c-In_2O_3 was easily lost oxygen atoms to form defective surface with oxygen vacancy [11,15,16]. These surface sites assist CO_2

activation and hydrogenation by stabilizing the key reaction intermediates, such as surface bound formate (HCOO), dioxymethylene (H_2COO), and H_2CO species; the hydrogenation of the latter gives surface methoxy species, supposedly *via* the rate-determining step [15,17]. H_2 can re-generate the vacancy which is replenished during methanol formation. This catalytic cycle may play an important role on the formation of methanol from CO_2 [12,18,19]. Due to the excellent CH_3OH selectivity of In_2O_3, CO_2 had been successfully hydrogenated to lower olefin through In_2O_3/SAPO-34 catalyst [10] and aromatic hydrocarbon through In_2O_3/HZSM-5 catalyst [14]. Except for CO_2 hydrogenation, c-In_2O_3 also can be used for methanol steam reforming, water-gas shift reaction, formaldehyde reforming and so on [20,21].

However, there is little knowledge about the intrinsic adsorption and catalytic property of rh-In_2O_3 except the electronic and structural characterization by theoretical calculations [13,22]. The prevalent scientific interest is the transition between these two phases as a case of ccp (cubic close-packed structure) to hcp (hexagonal closed-packed) transition at high-pressure and high-temperature condition [14,23,24]. As a meta-stability structure, rh-In_2O_3 was considered to be unstable at high temperature and pressure. However, Simon Penner *et al.* found rh-In_2O_3 remained stable over 430 ^oC in He or CO_2 atmospheres [25]. Thus stability of rh-In_2O_3 is satisfied for most of catalysis reactions. Rh-In_2O_3 have been proved that this nano-rhombodedra are terminated by (012) facets due to the geometric arrangement of face-sharing octahedral [26]. There is little information about the properties of surface chemistry, e.g. CO_2 hydrogenation activity, adsorption-desorption properties or reaction mechanisms.

Herein, the c-In_2O_3 and rh-In_2O_3 were synthesized for comparative study of CO_2 hydrogenation to elucidate the structure-activity relationship. The crystal phase of catalysts was characterized by X-ray diffraction (XRD) and shown in Fig. 1a. The diffraction peaks of black line were well matched with JCPDS No. 06-0416, which can be indexed to cubic bixbyite-type structure In_2O_3 (c-In_2O_3) [11]. Another diffraction pattern could be assigned to rhombohedral corundum-type (rh-In_2O_3), which was well matched with JCPDS 22-0336 [27]. There were no impurity peaks, indicating the single phase of the product. The average crystal size of c-In_2O_3 and rh-In_2O_3 calculated by Scherer equation in Fig. 1a were 19.8 and 24.5 nm, respectively.

During synthetic process, the difference between the catalysts was the solvent, *i.e.* methanol-based route for rh-In_2O_3 and water-based route for c-In_2O_3. As shown in Fig. 1b, $In(OH)_3$ was formed in the water-based route and then decomposed to c-In_2O_3 after calcination. In contrast, InOOH was formed in the methanol-based route and then rh-In_2O_3 was obtained after thermal decomposition of InOOH. During the calcination, the decomposition of $In(OH)_3$ was accompanied by water vapor and toward the stable phase. But for methanol-based route, InOOH with the residual methanol favored a transition coordination sphere of In^{3+} ions by avoiding fast hydrolysis and condensation, which evolved to the rhombohedral corundum-type [28,29]. The formation of precursors was critical for the successful synthesis of c-In_2O_3 and rh-In_2O_3. The rh-In_2O_3 was terminated by (012) plane and the presence of ammonia/methanol had strongly influence on the surface energy of the exposed facet [26]. However, the thermodynamically stable facet of c-In_2O_3 (110) face with surface energy of 0.969 J/m^2 was formed in the presence of water [11].

As Table S1 (Supporting information) and diagrammatic sketch (Figs. 1c and d) showed, c-In_2O_3 was Ia3 space group with lattice constant a = b = c = 10.126 Å and described as an oxygen-vacancy fluorite structure with O^{2-} anions missing in an ordered way [28]. There were two types of In^{3+} ions in c-In_2O_3 located at the end of a face-diagonal and a body-diagonal, which occupied octahedral and trigonal prismatic interstices of the O^{2-} anions [28,30]. The lattice parameters of rh-In_2O_3 with R3C space group were a = b = 5.491 Å and c = 14.526 Å. In comparison with c-In_2O_3, rh-In_2O_3 showed different atomic arrangement with a rather regular octahedron, including trigonal bi-prism coordinated In^{3+} with O^{2-} anions [26]. This structural difference was mainly due to the O^{2-} anions lattice change and In^{3+} ions shifted from octahedral and trigonal prismatic to trigonal bi-prism sites.

Raman was also conducted to understand the structural difference and the result was shown in Fig. 1e. The representative Raman spectra of the indium oxides (black line) was corresponded to c-In_2O_3. The peaks at 303, 495 and 629 cm^{-1} were associated with InO_6 octahedral, 133 and 363 cm^{-1} were associated with the bending vibrations of In_4O_4 and stretching vibrations of In-O-In [31]. Rh-In_2O_3 also exhibited the typical Raman-active phonons. The peaks at 161, 218 and 267 cm^{-1} were assigned to the symmetric stretching vibration of O-In-O, 377 cm^{-1} was the symmetric bending vibration of O-In-O [31]. The other frequencies were caused by the symmetric stretching and symmetric bending vibration of O-In-O [32].

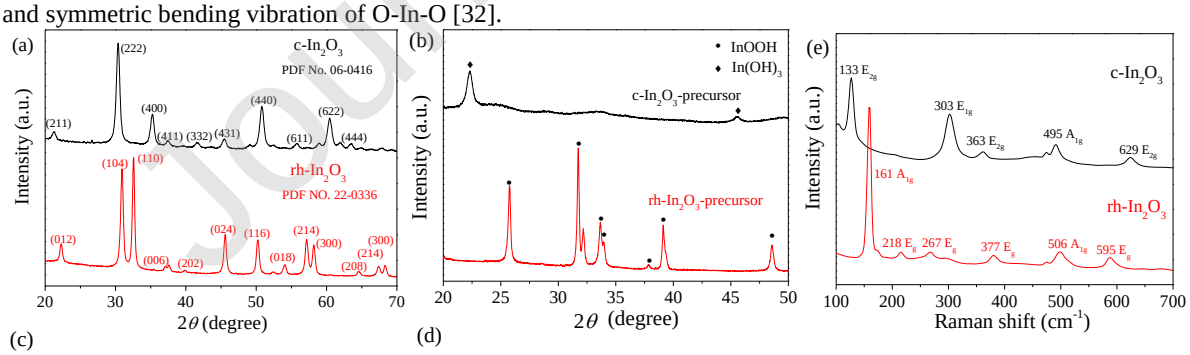

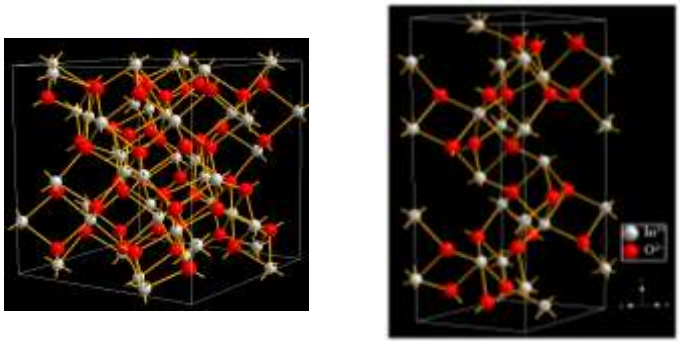

Fig. 1. Structural characterizations of c-In_2O_3 and rh-In_2O_3, (a) XRD, (b) XRD of precursor before calcination. Diagrammatic sketch of c-In_2O_3 (c) and (d) rh-In_2O_3, (e) Raman spectra.

Transmission electron microscopy (TEM) showed the average diameter of c-In_2O_3 and rh-In_2O_3 was around 17.9 nm and 24.9 nm, respectively. The summary of particle size distribution was showed in Fig. S1 (Supporting information). High resolution transmission electron microscopy (HRTEM) of c-In_2O_3 (Fig. S2 in Supporting information) exhibited the characteristic spacing of 0.505, 0.417 and 0.264 nm, corresponding to the (010), (211) and (104) faces of c-In_2O_3, respectively [33]. The spacing of 0.475 and 0.221 nm of rh-In_2O_3 (Fig. S2) well matched with the representative lattice distance of (211) and (222) faces of rh-In_2O_3 [32]. The selected area electron diffraction patterns were presented in Fig. S3 (Supporting information). In both catalysts, the discrete spots indicated well crystallinity and the distinct diffraction rings can be ascribed to many tiny crystallites.

X-ray photoelectron spectroscopy (XPS) was used to understand the surface chemical state and the results were enclosed in Fig. S4 (Supporting information). The binding energy was calibrated using C 1s energy of 285 eV in Fig. S5. As Fig. S4 showed, the broad and symmetric peak locked at 444.6 eV and 452.2 eV were belonged to In $3d_{5/2}$ and $3d_{3/2}$ of In_2O_3 [27,34]. Negligible binding energy value difference for both catalysts suggested similar surface chemical electronic property. O 1s core level of catalysts was composed of two components and the intensity was determined by curve fitting procedure. 530.1 eV can be assigned to lattice oxygen (O lattice) and 531.7 eV can be assigned to oxygen defect (O defect) [2]. This oxygen defects may be the sub-coordinated In atom that was activated by thermal calcination. The oxygen vacancy concentration was the fraction of surface oxygen atoms adjacent to a defect calculated from the de-convoluted O 1s XPS signal. It revealed that the oxygen vacancy amount of c-In_2O_3 (24.5%) was more than the amount of rh-In_2O_3 (21.2%).

The CO_2 hydrogenation performance was shown in Fig. 2. Both catalysts showed CO_2 catalytic activity and highly methanol selectivity at all tested temperatures. In addition to CH_3OH formation, these catalysts also generated CO as a primary byproduct (The detailed products information was enclosed in Fig. S6 in Supporting information). However, CO_2 conversion over catalysts under 300 °C was lower than 5% and gradually increased with reaction temperature increasing (Fig. 2a). Meanwhile, the selectivity of CH_3OH decreased and CO gradually became the dominate product, which was thermodynamically favorable with the increasing reaction temperature. In Fig. S6, the presence of CH_4 for c-In_2O_3 and absence for rh-In_2O_3 at high reaction temperature indicated the different hydrogenation ability. The hydrocarbon products of rh-In_2O_3 was merely methanol and c-In_2O_3 can further hydrogenate CO_2 to CH_4 at high temperature, suggesting higher hydrogenation ability of c-In_2O_3.

C-In_2O_3 showed higher CO_2 conversion than rh-In_2O_3. At 360 °C (Fig. 2a), CO_2 conversion of c-In_2O_3 was 17.02%, which was about three times higher than rh-In_2O_3. It was worthwhile mentioned that the specific surface area obtained from N_2-sorption (Fig. S7 in Supporting information) was 24.8 m^2/g for c-In_2O_3 and 22.8 m^2/g for rh-In_2O_3. The similar surface area for the two catalysts indicated that the catalytic difference was not the result of surface area. In addition, the rh-In_2O_3 showed higher methanol selectivity than c-In_2O_3. At 260 °C, the methanol selectivity of both catalysts were all over 80% and decreased gradually with the temperature increasing. Especially at 340 °C, the methanol selectivity of rh-In_2O_3 maintained approximate 30%. But the value of c-In_2O_3 was only 20%. As Table S2 showed, the two catalytic processes of methanol synthesis and methanol to hydrocarbon can combined into one integrated process and directly hydrocarbon molecule from CO_2 and H_2, which need >30% methanol selectivity at the optimized temperature over 340 °C [21]. Thus, both c-In_2O_3 and rh-In_2O_3 showed wide temperature range for high methanol selectivity and promising catalysts for hydrocarbon production coupling with zeolite catalysts. The apparent activation energy for CO_2 conversion was 55.33 and 55.39 kJ/mol over c-In_2O_3 and rh-In_2O_3, respectively in Fig. 2b. The quite close activation energy may indicate the same CO_2 hydrogenation mechanism, which was further confirmed by the following results of *in-situ* DRIFTS.

The space-time yield (STY) of methanol over the catalysts was also shown in Fig. 2c. C-In_2O_3 generated about 3.0 $mmol \cdot g^{-1} \cdot h^{-1}$ CH_3OH at 340 °C, which was higher than 1.8 $mmol \cdot g^{-1}$ h^{-1} of rh-In_2O_3. The stability of both catalysts showed slight deactivation after 12 h reaction on stream. The XRD patterns of used catalysts was shown in Fig. S8 (Supporting information). In compared with Fig. 1, the intensities of peaks in both catalysts were decreased. However, the diffraction peaks of both samples were still sharp and intense, indicating their highly crystalline nature. No impurity peaks were observed, confirming the high purity of the used catalysts. Moreover, the transformation between c-In_2O_3 and rh-In_2O_3 was not observed, which showed the structural stability under reaction condition. Moreover, the influence of experimental conditions on CH_3OH selectivity was also evaluated (Figs. 2d and e), which showed higher gas

hourly space velocity (GHSV) and pressure were beneficial for CH_3OH selectivity. And rh-In_2O_3 had higher CH_3OH selectivity during all experimental conditions.

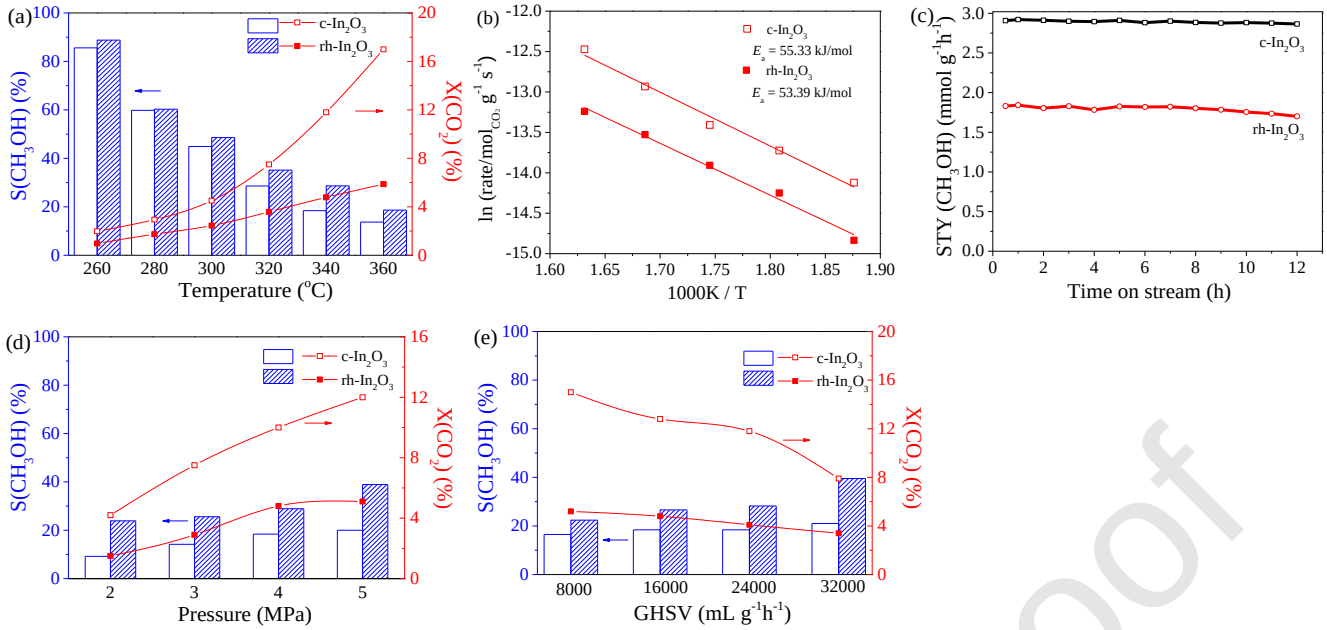

Fig. 2. Catalytic performance of the catalysts. (a) catalytic performance at the reaction temperatures from 260 °C to 360 °C with H_2/CO_2 = 4/1, 4 MPa, and 16,000 mL $g^{-1}\cdot h^{-1}$. (b) Arrhenius plot for CO_2 conversion. (c) Evolution of the methanol STY with time on stream. (d) The effect of pressure on CO_2 hydrogenation. The reaction condition: 340 °C, H_2/CO_2 = 4/1 and 16,000 mL· $g^{-1}\cdot h^{-1}$. (e) The effect of GHSV on CO_2 hydrogenation. The reaction condition: 340 °C, H_2/CO_2 = 4/1 and 4 MPa.

Temperature-programmed reduction (TPR) in hydrogen (H_2-TPR) was carried out to understand the reducibility of catalysts and the results were shown in Fig. 3a. Prior to the bulk reduction into metallic indium over 580 °C (c-In_2O_3) or 626 °C (rh-In_2O_3), there was one primary reduction peak [11,17]. The diverse reduction peak between c-In_2O_3 (212 °C) and rh-In_2O_3 (307 °C) was determined by the reducible oxygen atoms and exposing facets [35]. The reduction peak of rh-In_2O_3 mainly was associated with lattice oxygen atoms from (012) planes [27]. The reduction peak of c-In_2O_3 at 212 °C was associated with oxygen reduction from (110) planes [22,23]. Oxygen vacancy in In_2O_3-based catalysts was considered to be the active sites for CO_2 hydrogenation [11]. TPR profiles suggested that the oxygen of c-In_2O_3 was more active and easy to release than rh-In_2O_3. Thus, oxygen vacancy was easily generated in c-In_2O_3, which was linked with the CO_2 catalytic activity.

Temperature-programmed desorption (TPD) of CO_2 (CO_2-TPD) in Fig. 3b was used to understand the interaction between CO_2 and In_2O_3. CO_2 adsorbed as bicarbonate bridging two In atoms around oxygen vacancy sites and carbonate formed over oxygen atom [11,15,16,19]. Aside from the peak of physically adsorbed CO_2 appeared at approximately 100 °C, two additional peaks were observed in both catalysts. The desorption peaks at approximate 379 and 454 °C in c-In_2O_3 can be assigned to bicarbonate and carbonate, respectively. *In-situ* DRIFTS later found the transformation from bicarbonate to carbonate during heating-up. CO_2 desorption peaks of rh-In_2O_3 were appeared at 275 and 325 °C. Lower desorption temperature of rh-In_2O_3 suggested weaker basicity and interaction between CO_2 and rh-In_2O_3 than c-In_2O_3. Moreover, c-In_2O_3 with a large CO_2 desorption area featured higher density of adsorption sites. This strong and high density of basicity sites of c-In_2O_3 was conducive to enhance the CO_2 conversion.

The reason influenced the products selectivity can be explored by TPD experiment by using the main byproducts (CH_3OH and CO) as adsorbates 33. Before the TPD measurements, the samples were treated at 300 °C and then cooling to room temperature. CH_3OH was introduced through Ar bubbling at 60 °C and the adsorption procedure was last 2 h. As Fig. 3c showed, CH_3OH desorbed from rh-In_2O_3 was more difficult than c-In_2O_3 (peak at 384 °C versus 250 °C), suggesting stronger CH_3OH adsorption ability of rh-In_2O_3. In addition, the methanol adsorption area over rh-In_2O_3 was far larger than that of c-In_2O_3, which showed the more adsorptive sites for CH_3OH over rh-In_2O_3.

CO-TPD result was shown in Fig. 3d. c-In_2O_3 showed weak interaction with CO due to the absence of chemical desorption peak at high temperature except the physical desorption peak at about 100 °C. For rh-In_2O_3, there was a width desorption peak at about 432 °C aside from the physical adsorption peak. CO_2 hydrogenation experiments indicated higher CH_3OH selectivity of rh-In_2O_3 than c-In_2O_3, which could be partially explained by the results of by-products TPD experiment. For c-In_2O_3, CO was more easily desorbed from the surface than CH_3OH due to the weaker interaction between CO and c-In_2O_3. The rh-In_2O_3 showed CH_3OH desorbed at a lower temperature (384 °C and showed in Fig. 3c) than CO (432 °C and showed in Fig. 3d), which may be beneficial for CH_3OH selectivity improvement over rh-In_2O_3.

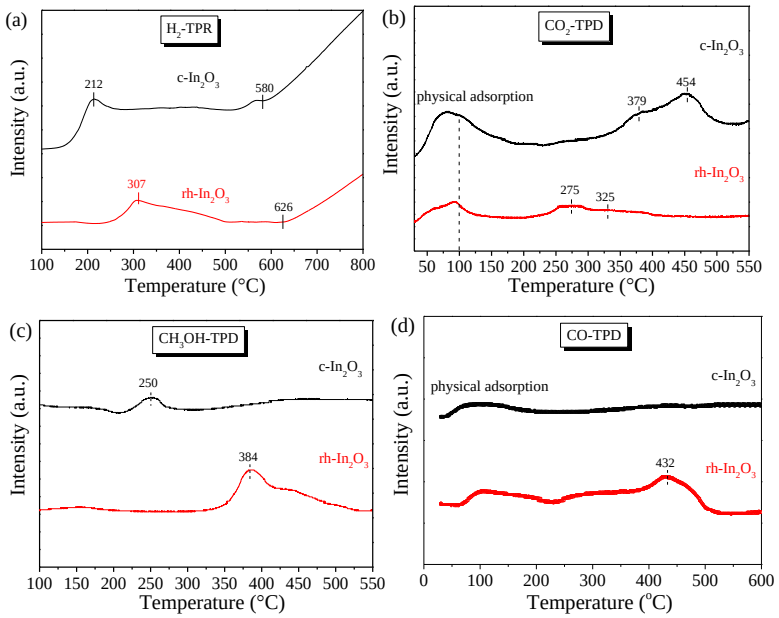

Fig. 3. Temperature programmed reduction and desorption of c-In_2O_3 and rh-In_2O_3. (a) H_2-TPR, (b) CO_2-TPD, (c) CH_3OH-TPD and (d) CO-TPD.

To further investigate the interaction between CO_2 and catalysts, *in-situ* DRIFTS experiment of CO_2 adsorption were carried out. It represented the characteristic peaks of adsorbed CO_2 on the surface at 40 °C and reaction intermediates along with the temperature increasing. There were three strong peaks located at 1356, 1420,1649 cm^{-1} and a weak peak at 1227 cm^{-1} (Fig. 4a and Table S3 in Supporting information). The intensity of these peaks gradually strengthened after 30 min exposure. In detail, the peak at 1649, 1420 and 1227 cm^{-1} could be identified as asymmetric stretching vibration ν_{as}(O-C-O), bending vibration δ(OH) and symmetric stretching vibration ν_s(O-C-O) of bicarbonate species (HCO_3^-) (as summarized in Table S1), respectively [36]. The other one at 1356 cm^{-1} can be assigned to ν_s(O-C-O) of carbonate (CO_3^{2-}) species and ν_{as}(O-C-O) of carbonate may hide or overlap in the peak shoulder of bicarbonate species (1400-1500 cm^{-1}). The surface of In_2O_3 contained lots of hydroxyl (-OH group) and easily reacted with CO_2 to form bicarbonate species as Scheme S1 (Supporting information) briefly illustrated [15,37].

Once reached 150 °C, it can be clearly seen that the vibration of bicarbonate weakened and the vibration of carbonate strengthened due to the ν_{as}(O-C-O) at 1501 cm^{-1} of carbonate appeared. This transformation meant bicarbonate turned to carbonate and was significantly enhanced until bicarbonate disappeared as the temperature up to 300 °C. Meanwhile, a new peak at 2077 cm^{-1} that assigned to adsorbed CO species appeared [25]. This CO species suggested CO_2 can be directly reduced to CO by In_2O_3. This result was consistent with the Density Functional Theory（DFT) simulation of previous reports, which indicated CO_2 reacted with -OH on the In_2O_3 surface to form a bicarbonate specie [15,16]. CO_2 gradually turned to CO and leaved O atom quenching the oxygen vacancy, which could be regenerated by hydrogen or thermal treatment, as the temperature increased. The similar adsorption and transformation phenomena could be also found in rh-In_2O_3 (Fig. 4b and Table S3). It was worthwhile mentioned that the intensity of carbonate for rh-In_2O_3 was much lower and even disappeared at 300 °C compared to c-In_2O_3, which was consistent with the weak interaction between CO_2 and rh-In_2O_3 resulted from CO_2-TPD experiments.

There was an urgent need but it was a significant challenge to directly study the reaction between H_2 or CO_2/H_2 and In_2O_3 by *in-situ* DRIFTS. Because the interaction of In_2O_3 with H_2 strongly decreased the IR diffuse reflection and disturbed the surface stability (Fig. S9 in Supporting information), which prevented the reliable study by *in situ* DRIFTS [11,38,39]. Thus, the indirect strategy of HCOOH reaction was usually adopted instead. The mechanism of methanol synthesis from CO_2 hydrogenation on the In_2O_3 surface was formate-path as the previous reports, which meant CO_2 firstly hydrogenation to formate ($HCOO^-$) and subsequently to methoxy and CH_3OH [11,15,16,33]. The interaction of formate and catalysts can be used to indirectly testify CO_2 hydrogenation mechanism.

After treatment with formic acid and Ar sweeping at 40 °C, c-In_2O_3 showed typical stretching vibration of formate species in Fig. 4c. The characteristic absorption bands at 1619, 1563, 1384 and 1359 cm^{-1} can be assigned to formate [40]. The band at 1359 cm^{-1} was ν_s (O-C-O) vibration and 1384 cm^{-1} was δ (CH) characteristic vibration of formate species [40]. 1619 and 1563 cm^{-1} were ν_{as} (O-C-O) vibration which indicated different adsorption sections of formate species, *i.e.* 1619 cm^{-1} was characteristic of the vibration of unsymmetrical formate and 1563 cm^{-1} was the symmetrical bidentate formate [40], as illustrated in Scheme S2 (Supporting information).

Further investigation explored the temperature dependence of the surface coverage with unsymmetrical and symmetrical bidentate formate species. At 100 °C, the adsorption bands of unsymmetrical formate species at 1619 cm^{-1} decreased. On the contrary, the symmetrical bidentate formate species at 1563 cm^{-1} enhanced. This opposite change for these formates on the surface could be indicative of the transformation of unsymmetrical to symmetrical bidentate formate species. The unsymmetrical formate was metastable state and easily changed to symmetrical bidentate formate under thermal treatment [41].

When temperature increased to 200 °C, the unsymmetrical bidentate formate became obscured and symmetrical bidentate formate remained stable. The band at 1171 cm^{-1} can be assigned to ν(C-O) of methoxy (CH_3O) species, 1730 cm^{-1} assigned to ν(C=O) vibration

of aldehyde and the other two bands between 2300-2400 assigned to CO_2 gas phase [42,43]. These new bands became stronger and the HCOO species vanished as the temperature increased to 250 °C. These new species suggested the formate transformation on c-In_2O_3, which contained decomposition and hydrogenation reaction. Aldehyde and carbon dioxide were decomposed from formate species. The hydrogen was generated from the reaction between In-H and proton of formic acid gas (Scheme S2) [44]. Methoxyl, which was apparently as the precursor of methanol, may come from the hydrogenation of HCOO species.

As for rh-In_2O_3, it was easily found the bands were similar to c-In_2O_3 in spite of some peaks shift in Fig. 4d. The peak position of all bands were summarized in Table S4 (Supporting information). At 250 °C, the formate species on rh-In_2O_3 was completely disappeared and even formed the negative spikes, suggesting that formic acid was easily decomposed over rh-In_2O_3. Overall, the oxygen vacancy on the In_2O_3 surface assists CO_2 activation and hydrogenation and also stabilized the key intermediates involved in methanol formation. In addition, methanol formation replenishes the oxygen vacancy sites whereas H_2 helps to generate the vacancies. The cycle between the perfect and defective states of the surface catalyzes the formation of methanol from CO_2 hydrogenation [15,16].

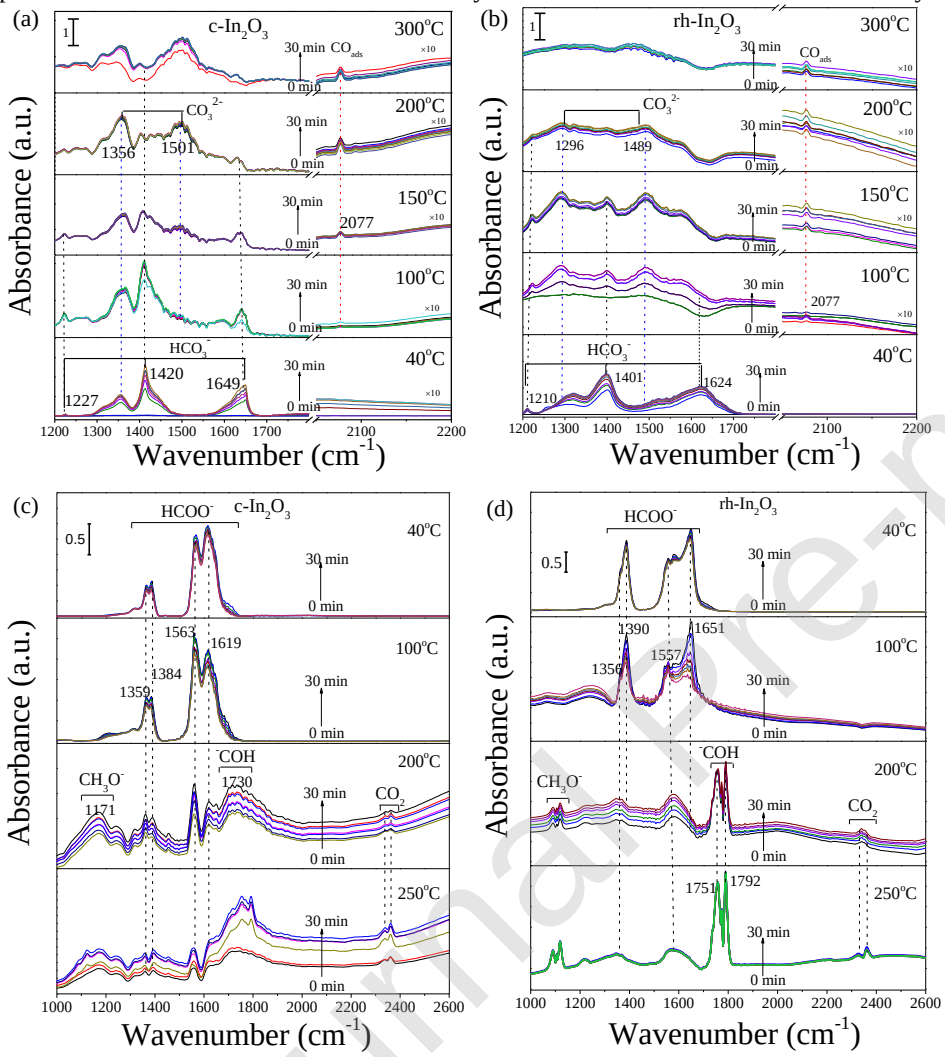

Fig. 4. *In-situ* DRIFTS spectra of CO_2 adsorption and conversion over the catalysts, (a) c-In_2O_3 and (b) rh-In_2O_3. HCOOH adsorption and conversion over the catalysts, (c) c-In_2O_3 and (d) rh-In_2O_3

In_2O_3 showed significant advantage in CH_3OH synthesis at high temperature. The active sites of In_2O_3 catalyst was ascribed to oxygen vacancy sites under reaction conditions. These surface sites assisted CO_2 activation and hydrogenation by stabilizing the key reaction intermediates, such as surface bound formate (HCOO), and further hydrogenation to CH_3OH. This mechanism suggested that oxygen vacancy sites could be replenished during CO_2 hydrogenation. As a reducible oxide, In_2O_3 was different from conventional binary or ternary metal-metal oxide catalysts. CO_2 activation, H_2 activation and CH_3OH synthesis can be completed by In_2O_3, not the combination or interface of metal-metal oxide catalysts. This feature successfully restrained the CO formation and enhanced the CH_3OH selectivity. Both c-In_2O_3 and rh-In_2O_3 catalysts showed catalytic activity and thermal stability at high reaction temperature. And the activation energy and reaction mechanism of CO_2 hydrogenation was identical. The results of *in-situ* DRIFTS showed CO can be directly generated from CO_2 on the surface of In_2O_3. This redox reaction was not sustainable because the oxygen vacancy was gradually vanished by CO_2. So the cyclic creation and annihilation of oxygen vacancy was necessary for the continuous methanol formation from CO_2 hydrogenation. The intermediate formate was used to indirectly explore the reaction mechanism, which showed formate can decompose to CO_2 and

hydrogenate to CH_3OH. Meanwhile, the absence of CO signal may be ascribed to its very low concentration, indicating the generation of CO from formate can be well restrained on In_2O_3. The oxygen vacancy on the In_2O_3 were beneficial for CO_2 activation and stabilization of the key intermediates. CH_3OH generation replenished the oxygen vacancy and H_2 regenerated the vacancy to achieve the catalytic cycle. Thus, the generation of CO and CH_3OH on the surface of In_2O_3 can separate to two pathways that redox-path reaction from CO_2 to CO and formate-path reaction from CO_2 to CH_3OH. CO_2 and H_2 favored to form formate and then hydrogenation to CH_3OH on the surface of In_2O_3, suggesting the high CH_3OH selectivity.

However, due to the thermodynamic restrictions, CO still was the main product at high temperature. With the higher reducibility and basicity, c-In_2O_3 showed higher CO_2 conversion and CH_3OH productivity than rh-In_2O_3. And the adsorbed CH_3OH molecules desorbed at lower temperature than that of the adsorbed CO molecules on rh-In_2O_3. In contrast, CO was more easily desorbed from the surface than CH_3OH on c-In_2O_3. So the rh-In_2O_3 showed higher CH_3OH selectivity during CO_2 hydrogenation compared with the c-In_2O_3.

Above all, the comparative study of c-In_2O_3 and rh-In_2O_3 for CO_2 hydrogenation was carried out. C-In_2O_3 showed higher CO_2 conversion activity than rh-In_2O_3, which was ascribed to the higher reducibility and basicity within c-In_2O_3 and associated with the generation of the oxygen vacancy. rh-In_2O_3 showed higher methanol selectivity than c-In_2O_3. Although different structures showed different CO_2 hydrogenation performance, the hydrogenation mechanism was identical for the two catalysts. CO_2 can be directly reduced to CO through redox mechanism and CO_2 hydrogenation to CH_3OH was through formate-path. This work demonstrated the fundamental understanding of the structure-activity relationship for rh-In_2O_3 and c-In_2O_3 catalysts and offered some hint for superior catalytic system for CO_2 hydrogenation with high CH_3OH selectivity over 340 ºC.

Declaration of interests

☑The authors declare that they have no known competing financial interests or personal relationships that could have appeared to influence the work reported in this paper.

Acknowledgements

The work was financially supported by the National Natural Science Foundation of China (No. 21878116) and Natural Science Foundation of Hubei Province (No. 2019CFA070). The authors thank the Analysis and Testing Center of Huazhong University of Science and Technology for analytical support.

References

[1] S. Li, Y. Wang, B. Yang, L. Guo, Appl. Catal. A 571 (2019) 51-60.
[2] B. Yang, L. Wang, Z. Hua , L. Guo, Ind. Eng. Chem. Res. 58 (2019) 9838-9843.
[3] B. Yang, W. Deng, L. Guo, T. Ishihara, Chin. J. Catal., 41 (2020), 1348-1359;
[4] R.W. Dorner, D.R. Hardy, F.W. Williams, H.D. Willauer, Energy Environ. Sci. 3 (2010) 884.
[5] Z. Li, J. Wang, Y. Qu, et al., ACS Catal. 12 (2017) 8544-8548.
[6] J. Wei, Q. Ge, R. Yao, et al., Nat. Commun. 8 (2017) 15174.
[7] L. Qi, Y. Wei, L. Xu, Z. Liu, ACS Catal. 5 (2015) 3973-3982.
[8] X. Zhu, J.P. Hofmann, B. Mezari, et al., ACS Catal. 6 (2016) 2163-2177.
[9] K.Cheng, B.Gu, X.Liu, et al., Angew. Chem., Int. Ed. 55 (2016) 4725-4728.
[10] P. Gao, S. Dang, S. Li, et al., ACS Catal. 8 (2017) 571-578.
[11] O. Martin, A.J. Martin, C. Mondelli, et al., Angew. Chem., Int. Ed. 55 (2016) 6261-6265.
[12] M.S. Frei, C. Mondelli, R. García-Muelas, et al., Nat. Commun. 10 (2019) 3377.
[13] J.M. Yang, Z.P. Qi, Y.S. Kang, L. Qing, W. Sun, Chin. Chem. Lett. 27 (2016) 492-496.
[14] P. Gao, S. Li, X. Bu, et al., Nat. Chem. 9 (2017) 1019-1024.
[15] A. Tsoukalou, P. Abdala, D. Stoian, et al., J. Am. Chem. Soc. 141 (2019) 13497−13505.
[16] M.F. Bekheet, M.R. Schwarz, S. Lauterbach, et al., Angew. Chem., Int. Ed. 52 (2013) 6531-6535.
[17] A. Gurlo, Angew. Chem. Int. Ed. 49 (2010) 5610-5612.
[18] T. Bielz, H. Lorenz, P. Amann, B. Klötzer, S. Penner, J. Phys. Chem. C 115 (2011) 6622-6628.
[19] J. Wang, H. Wang, P. Hu, Sci. China: Chem. 61 (2017) 336-343.
[20] S. Shu, D. Yu, Y. Wang, et al., J. Cryst. Growth 312 (2010) 3111-3116.
[21] E.M. Kock, M. Kogler, C. Zhuo, et al., Phys. Chem. Chem. Phys. 19 (2017) 19407-19419.
[22] J. Ye, C. Liu, D. Mei, Q. Ge, ACS Catal. 3 (2013) 1296-1306.
[23] J. Ye, C. Liu, Q. Ge, J. Phys. Chem. C 116 (2012) 7817-7825.
[24] N. Rui, Z. Wang, K. Sun, et al., Appl. Catal. B 218 (2017) 488-497.
[25] M. Neumann, D. Teschner, A. Knop-Gericke, W. Reschetilowski, M. Armbrüster, J. Catal. 340 (2016) 49-59.
[26] J. Ye, Q. Ge, C. Liu, Chem. Eng. Sci. 135 (2015) 193-201.
[27] A. Gurlo, S. Lauterbach, G. Miehe, H. Kleebe, R. Riedel, J. Phys. Chem. C 112 (2008) 9209-9213.
[28] K. Reyes-Gil, E. Reyes-García, D. Raftery, J. Phys. Chem. C 111 (2007) 14579-14588.
[29] M. Epifani , P. Siciliano , A. Gurlo, N. Barsan, U. Weimar, J. Am. Chem. Soc. 126 (2004) 4078-4079.
[30] A. Gurlo, G. Miehe, R. Riedel, Chem. Commun. 19 (2009) 2747-2749.
[31] A. Gurlo, P. Kroll, R. Riedel, Chem.-Eur. J. 14 (2008) 3306-3310.
[32] J.A. Sans, R. Vilaplana, D. Errandonea, et al., Nanotechnology 28 (2017) 205701.
[33] D. Yu, S. Yu, S. Zhang, et al., Adv. Funct. Mater. 13 (2003) 497-501.
[34] M.S. Frei, M. Capdevila-Cortada, R. García-Muelas, et al., J. Catal. 361 (2018) 313-321.
[35] W. Yin, D. Esposito, S. Yang, et al., J. Phys. Chem. C 114 (2010) 13234-13240.
[36] F. Liao, Y. Huang, J. Ge, et al., Angew. Chem., Int. Ed. 50 (2011) 2162-2165.
[37] J.C. Matsubu, S. Zhang, L. DeRita, et al., Nat. Chem. 9 (2017) 120-127.

[38] T. Bielz, H. Lorenz, W. Jochum, et al., J. Phys. Chem. C 114 (2010) 9022-9029.
[39] E.M. Köck, M. Kogler, M. Grünbacher, et al., J. Phys. Chem. C 120 (2016) 15272-15281.
[40] G. Popova, T. Andrushkevich, Y. Chesalov, E. Stoyanov, Kinet. Catal. 41 (2000) 805-811.
[41] S. Kattel, B. Yan, Y. Yang, J.G. Chen, P. Liu, J. Am. Chem. Soc. 138 (2016) 12440-12450.
[42] S.V. Ryazantsev, V.I. Feldman, L. Khriachtchev, J. Am. Chem. Soc. 139 (2017) 9551-9557.
[43] K. Larmier, W.C. Liao, S. Tada, et al., Angew. Chem., Int. Ed. 56 (2017) 2318-2323.
[44] S.T. Teklemichael, M.D. McCluskey, J. Phys. Chem. C 116 (2012).